

Good Noise Makes Good Edits: A Training-Free Diffusion-Based Video Editing with Image and Text Prompts

Saemee Choi*
KAIST

saemee99@kaist.ac.kr

Sohyun Jeong*
KAIST

jsh0212@kaist.ac.kr

Hyojin Jang
KAIST

wkdgywlsrud@kaist.ac.kr

Jaegul Choo
KAIST

jchoo@kaist.ac.kr

Jinhee Kim
KAIST

seharanul17@kaist.ac.kr

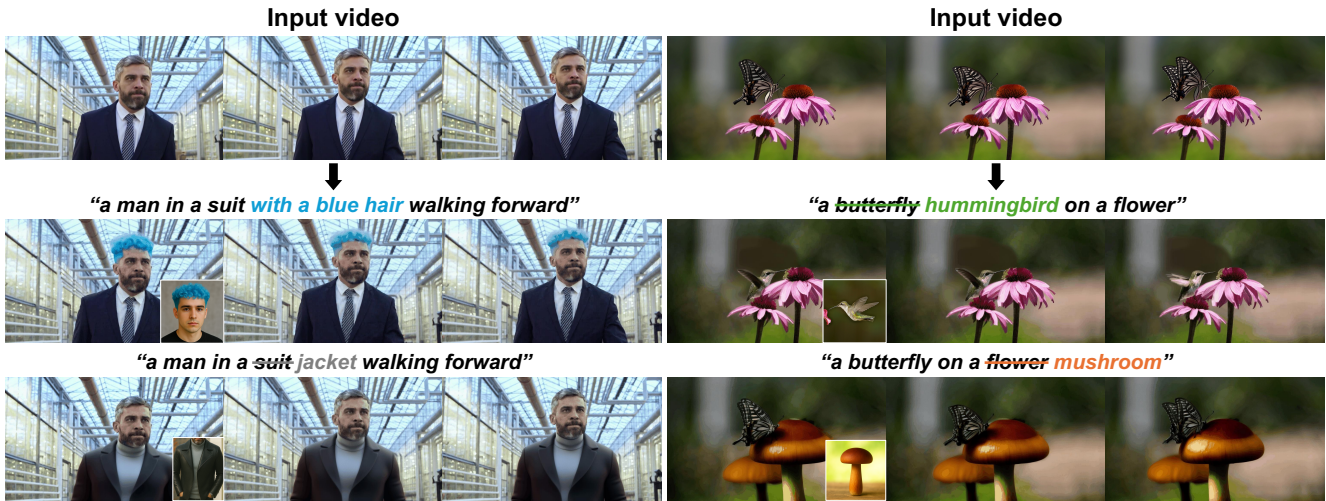


Figure 1. **Qualitative results of VINO.** Our training-free method, VINO, successfully achieves video edits using text and image prompts.

Abstract

We propose **VINO**, the first **zero-shot, training-free** video editing method conditioned on both image and text. Our approach introduces ρ -start sampling and dilated dual masking to construct structured noise maps that enable coherent and accurate edits. To further enhance visual fidelity, we present zero image guidance, a controllable negative prompt strategy. Extensive experiments demonstrate that VINO faithfully incorporates the reference image into video edits, achieving strong performance compared to state-of-the-art baselines, all without any test-time or instance-specific training.

1. Introduction

Diffusion-based video editing methods have shown notable achievements in recent years, enabling precise modifications

of objects in videos based on user prompts [5, 8, 25, 26, 49, 52]. Primarily, text-driven video editing models have gained considerable attention for their ability to modify video content while maintaining temporal consistency [11, 23, 30, 42]. These methods have demonstrated impressive results across a wide range of applications, such as appearance editing [5, 8, 21, 23], and style transfer [9, 11, 45, 49].

However, text-based video editing has inherent limitations, particularly when modifying objects with intricate and unique details, where textual descriptions alone are often insufficient to precisely convey the desired attributes (Fig. 2(a)). Moreover, crafting detailed textual prompts is cumbersome, requiring extensive trial-and-error to achieve the intended modifications. This challenge becomes even more pronounced when the editing method necessitates one-shot finetuning for each edit [23, 30, 37].

To mitigate the need for costly text prompt engineering, recent work has explored video editing methods guided by both image and text. However, such approaches [14, 50]

*Equal contribution



Figure 2. **Importance of appropriate integration of image prompts in video editing.** Given (a) a source video, we compare (b) a state-of-the-art text-driven video editing method, (c) a naive combination of a pretrained T2V model with an image-guided module, and (d) our proposed method. The text-only approach in (b) struggles to accurately transfer the structural appearance of the car in the reference image. Simply attaching the image-guided module to a pretrained T2V model, as in (c), produces unnatural results. In contrast, our proposed training-free method in (d) precisely transfers the car in the reference image into the video with high fidelity.

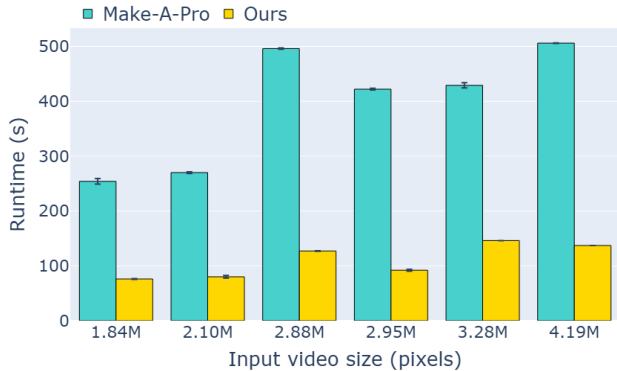


Figure 3. **Runtime comparison across video resolutions.** We compare VINO with Make-A-Pro [50], an image-guided video editing method. Results are averaged over three runs per setting.

suffer from weakened temporal consistency and require per-video finetuning, making them unsuitable for real-world editing scenarios. Other approaches employ additional guidance such as user-defined semantic keypoints alongside image and text prompts [12, 39] to achieve more precise control. While effective for temporally coherent local editing guided by reference images, these methods require substantial user interaction and additional training, limiting their practicality.

Therefore, we propose **Video editing with Noise control (VINO)**, the first zero-shot, training-free video editing framework conditioned on both image and text prompts. As illustrated in Fig. 1, our method enables localized video edits guided by reference images, without any additional training or cumbersome user interaction.

We leverage recent advances in the image domain to enable high-fidelity video editing without finetuning. In particular, pretrained image encoders and adapters [7, 19, 44, 46]

have shown success in injecting reference features into cross-attention layers. However, directly connecting these image-based techniques to existing text-to-video (T2V) models produces unnatural results, pasting the reference image onto the video without considering the source video’s layout (Fig. 2(c)). We address this semantic unnaturalness by introducing ρ -start sampling inspired by [24], which starts DDPM sampling from intermediate time steps to generate realistic images from stroke paintings. In our strategy, both DDIM sampling and inversion begin from intermediate time steps, preserving the layout and motion of the source video.

While this strategy effectively balances the appearance of the reference and the layout of the source, it still struggles when replacing source objects with targets of significantly different sizes or shapes (Fig. 7(a)). To overcome object size and shape discrepancies, we design VINO with a two-stage dilated dual masking strategy. In the first stage, we apply dilated masking to blend source video latents with editing latents during the sampling process, producing a coarse edited video. In the second stage, this coarse edited video is refined using dilated dual masking, enabling more flexible spatial blending for accurate appearance transfer.

We further present zero-image guidance to address occasional color desaturation. This controllable negative prompt strategy steers generation away from the zero-image direction, thereby improving color fidelity. Consequently, our method achieves high visual quality and temporal consistency (Fig. 2(d)), while offering clear efficiency advantages over methods requiring finetuning (Fig. 3).

In summary, our key contributions are:

- We propose **VINO**, the first zero-shot video editing method using both text and image prompts, preserving motion and temporal consistency without training.
- We introduce a noise map construction strategy including

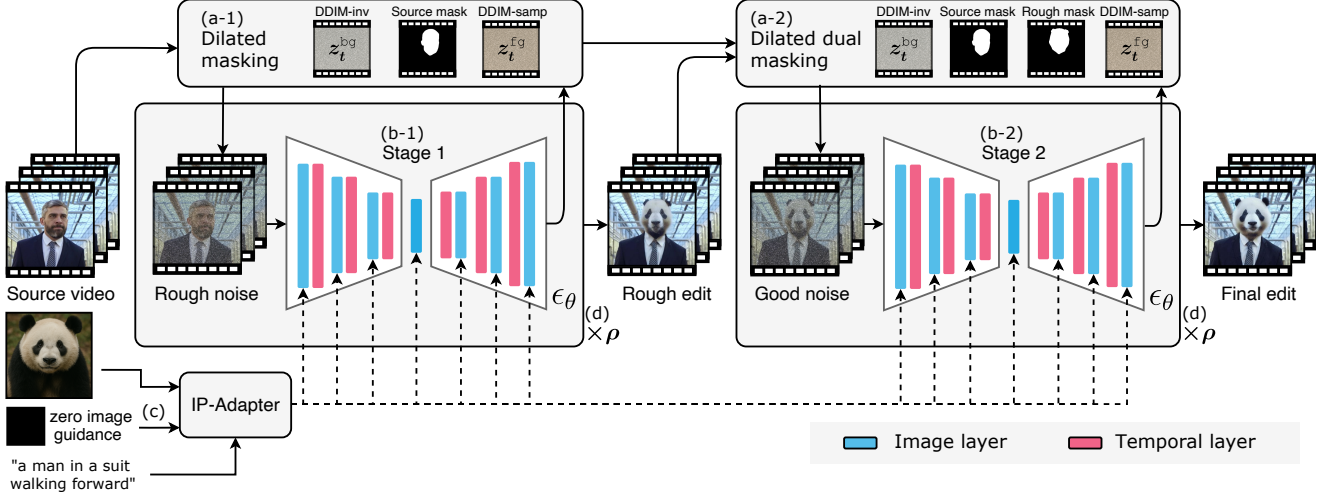


Figure 4. **Overview of VINO.** Our proposed training-free approach, VINO, adopts a coarse-to-fine scheme to guide the two-stage editing process via strategically designed noise maps. Both stages leverage ρ -start sampling with text and image prompts. In the first stage, a rough noise map is constructed from the source video via dilated masking (a-1), which is then denoised by the pretrained T2V model to yield a rough edit (b-1). In the second stage, a refined *good noise* map is derived from the rough edit via dilated dual masking (a-2). Finally, the model produces the final output based on this *good noise* map (b-2), faithfully reflecting the prompts while preserving motion and structure.

ρ -start sampling to preserve the motion patterns and spatial layout of the source video, and dilated dual masking to ensure smooth appearance transfer.

- We present zero image guidance, enhancing color saturation via controllable negative prompt blending.
- Comprehensive quantitative and qualitative evaluations demonstrate that our method outperforms existing state-of-the-art approaches in both quality and efficiency.

2. Methods

We introduce **VINO**, a training-free video editing approach that performs object replacement while maintaining overall scene coherence using text and image prompts, as illustrated in Fig. 4. Our method is grounded in the careful integration of well-structured noise with appropriately chosen components. Specifically, we consider two key ingredients: the foreground latent, obtained via ρ -start sampling, and the background latent, acquired through DDIM inversion of the source video. These latents are blended using a tailored mask derived from both the source and target object masks, employing dilated dual masking to ensure smooth transitions and spatial consistency. In addition, we apply zero image guidance, a negative prompt-based strategy, to enhance color saturation and overall visual fidelity in the final output.

2.1. Preliminaries

Latent Diffusion Models (LDMs). LDMs [34] perform the diffusion process in a compressed latent space obtained from an autoencoder \mathcal{E}, \mathcal{D} . Given an input image x , the encoder produces a clean latent representation $z_0 = \mathcal{E}(x)$,

where the diffusion process adds and removes noise as:

$$z_t = \sqrt{\alpha_t} z_0 + \sqrt{1 - \alpha_t} \epsilon, \quad \epsilon \sim \mathcal{N}(0, \mathbf{I}). \quad (1)$$

To balance realism and prompt adherence, classifier-free guidance [16] combines conditional and unconditional diffusion model predictions as follows:

$$\hat{\epsilon}_\theta = (1 + w)\epsilon_\theta(z_t, t, c) - w\epsilon_\theta(z_t, t, \bar{c}), \quad (2)$$

where w is the guidance scale, c is the conditioning input, and \bar{c} denotes the negative conditioning input. This design enables efficient training and sampling while maintaining high-quality visual fidelity consistently.

DDIM Sampling and Inversion. DDIM [36] provide a deterministic and efficient sampling process that reduces the number of steps required for faithful generation. The sampling process updates the latent as:

$$z_{t-1} = \sqrt{\alpha_{t-1}} \left(\frac{z_t - \sqrt{1 - \alpha_t} \epsilon_\theta(z_t, t)}{\sqrt{\alpha_t}} \right) + \sqrt{1 - \alpha_{t-1}} \cdot \epsilon_\theta(z_t, t), \quad (3)$$

where we denote this update rule as $\text{DDIM-samp}(z_t, t)$. The inversion process can be obtained by reversing these sampling steps, enabling reconstruction and fine-grained editing in the latent space. For editing, specific regions can be modified by blending DDIM inversion latents from the source and ongoing edit using a spatial mask:

$$z'_t = z_t^{\text{fg}} \odot M + z_t^{\text{bg}} \odot (1 - M), \quad (4)$$

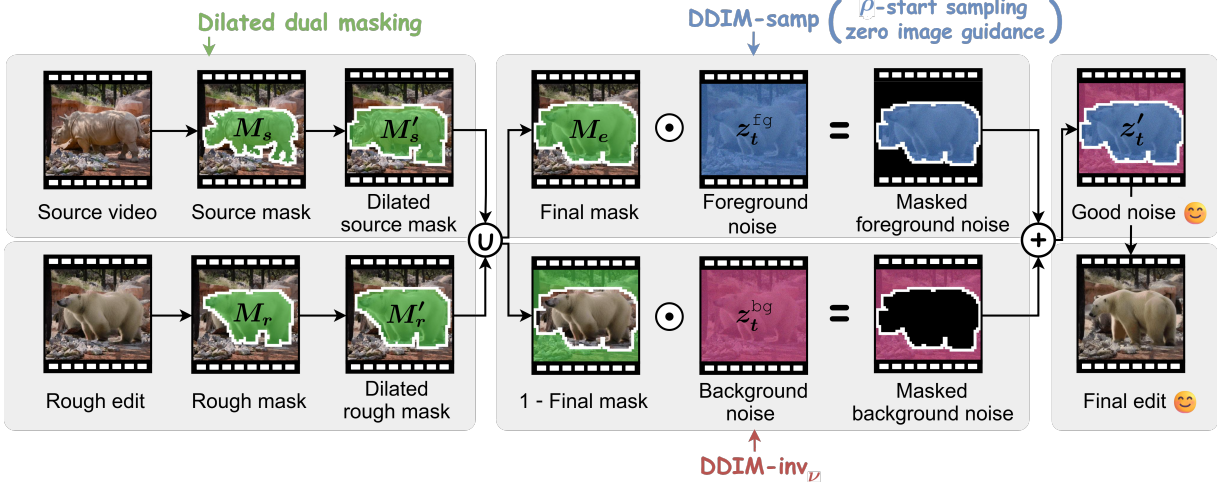


Figure 5. **Controlled noise sampling for structured edits in VINO.** Foreground and background latents, obtained via ρ -start sampling and zero image guidance, are blended using a final mask formed by the union of dilated source and target masks. This enables clean removal of the source object and seamless insertion of the target.

where M specifies the edited region, z_t^{fg} and z_t^{bg} denote background and foreground latents, respectively.

2.2. Overview

Given a source video $\mathcal{V}_s \in \mathbb{R}^{F \times C_s \times H_s \times W_s}$, our goal is to edit the foreground object and generate an edited video $\mathcal{V}_e \in \mathbb{R}^{F \times C_s \times H_s \times W_s}$, guided by a reference image $\mathcal{R} \in \mathbb{R}^{C_r \times H_r \times W_r}$ and a text prompt \mathcal{T} , while preserving the original background and motion dynamics. Here, F is the number of frames, C_s is the number of source video channels, and H_s and W_s are the height and width of each frame. Similarly, C_r , H_r , and W_r represent the channel and spatial dimensions of the reference image.

Our approach achieves this goal through a two-stage editing pipeline, as shown in Fig. 4. In the first stage, we construct a rough noise to enable localized object modification. In the second stage, this rough noise is refined into a more well-structured *good noise*, leading to higher-fidelity editing.

2.3. How to construct a good noise for video editing?

We first encode the source video \mathcal{V}_s into the latent space using a pretrained VAE encoder \mathcal{E} . We then initialize the noisy latent using ρ -start sampling (Section 2.3.2), a modification of the DDIM sampling schedule, which enables better preservation of the source video’s structure and motion. This noisy latent is passed into a pretrained T2V diffusion model ϵ_θ where we incorporate both image and text guidance using the IP-Adapter [46]. The image and text features from CLIP image encoder CLIP_{img} and CLIP text encoders CLIP_{txt} [31] are injected into each corresponding cross-attention layers of the T2V model as condition embeddings:

$$c_{\text{img}} = \text{CLIP}_{\text{img}}(\mathcal{R}) \quad \text{and} \quad c_{\text{txt}} = \text{CLIP}_{\text{txt}}(\mathcal{T}), \quad (5)$$

In addition, negative guidance using \bar{c}_{img} and \bar{c}_{txt} , which denote the negative image and text embeddings respectively, helps suppress irrelevant visual or textual features.

During the denoising process with condition embeddings, we employ a foreground-background separation mechanism to perform object-centric modifications while preserving background fidelity, inspired by latent blending [1, 2, 12, 14]. Specifically, we split the noisy latent z_t into foreground and background regions using the object segmentation mask M . For the background region, we retrieve the DDIM inversion noise corresponding to the current time step to preserve the background of the source video \mathcal{V}_s . In contrast, the foreground region is denoised by iteratively updating the noisy latent from the previous time step using a denoising network ϵ_θ , guided by the condition embeddings. This enables the foreground object to be progressively edited to resemble the target object. Formally, the foreground latent z_t^{fg} and background latent z_t^{bg} at time step t are computed as:

$$z_{t-1}^{\text{fg}} = \text{DDIM-samp}(z_t', c_{\text{img}}, c_{\text{txt}}, \bar{c}_{\text{img}}, \bar{c}_{\text{txt}}, t), \quad (6)$$

$$z_{t-1}^{\text{bg}} = z_{t-1}, z_{t-1} \in \{z_t\}_{t=1}^{\tau_v} \text{ from DDIM-inv}(z_0). \quad (7)$$

We then blend these two latents using M via our dilated dual masking (see Section 2.3.1), as follows:

$$z'_{t-1} = z_{t-1}^{\text{fg}} \odot M + z_{t-1}^{\text{bg}} \odot (1 - M), \quad (8)$$

where \odot denotes element-wise multiplication. We use different mask M at each stage. Specifically, in the first stage, the dilated source mask from the source video, $M'_s \in \mathbb{R}^{F \times C_s \times H_s \times W_s}$, is used. Through the denoising process in the first stage, we obtain a roughly edited video \mathcal{V}_r , which reflects the general structure and appearance of the target

object. However, this rough edit may still retain residual features of the source object, which should be removed for a clean visual transformation ultimately.

To address the limitations of single mask blending, we introduce a second stage that further refines the output. In this stage, we generate the final mask M_e by combining the initial mask M'_s with the rough mask M'_r derived from the rough edit. Foreground latent z_t^{fg} and background latent z_t^{bg} are regenerated from the rough edit \mathcal{V}_r using the same procedure as in the first stage. With the final mask and the regenerated latents, we construct a more refined noise map, which we refer to as *good noise*. It is designed to erase the original object and accurately follow the shape of the new object while maintaining the background. After denoising steps in the second stage, latents are decoded using the pretrained VAE decoder \mathcal{D} to generate the final output. Note that the entire pipeline is training-free, relying solely on pretrained models for mask extraction and video generation.

2.3.1. Dilated dual masking

Our proposed method coordinates structured noise to define editable regions in each frame and enables selective editing of target objects (Fig. 5). Unlike Blended Latent Diffusion (BLD) [1], which gradually shrinks masks during diffusion to address resolution degradation, our dilated dual masking uses a fixed dilation to refine boundaries and better spatially align source–target shapes.

In the first stage, only the source object mask M_s is available, which roughly outlines the foreground region to be edited (Fig. 4(b-1)). However, this mask lacks contextual adaptation to the background, often resulting in sharp edges and unnatural transitions at the object boundaries. Thus, we apply morphological dilation to smooth boundaries and facilitate seamless object replacement (Fig. 4(a-1)). Specifically, a single-iteration morphological dilation is applied to a binary matrix M with a kernel of size $k \times k$. For each pixel position (p, q) , the output value is determined as the maximum value within a neighborhood defined by \mathcal{N}_k , where $\mathcal{N}_k = \{(i, j) \mid -r \leq i, j \leq r\}$ and $r = \lfloor \frac{k}{2} \rfloor$. The dilation operation is formally expressed as:

$$M'[p, q] = \max_{(i, j) \in \mathcal{N}_k} M[p + i, q + j]. \quad (9)$$

As a result, the dilated source mask M'_s is used to blend latents in Eq. 8 to produce rough edits \mathcal{V}_r .

In the second stage, we similarly obtain the dilated rough mask M'_r from the rough edits \mathcal{V}_s (Fig. 4(b-2)). However, blending foreground and background latents using either the dilated source mask M'_s or the dilated rough mask M'_r poses the risk that parts of the source video may remain visible or that the generation area for the target object may not be fully covered. To address this, we leverage masks from both the first and second stages (Fig. 4(a-2)). The final mask M_e is computed as the union of the dilated source mask M'_s and

the dilated rough mask from the first stage M'_r , as shown in the following equation below:

$$M_e = M'_s \cup M'_r. \quad (10)$$

Finally, we construct the *good noise* z'_t using the final mask M_e to guide the final blending process in Eq. 8. This enables the second stage to generate more realistic, artifact-free results, as M_e precisely defines the edited region. In particular, it ensures clean removal of the original object, accurate reflection of the new object’s shape, and consistent preservation of the background appearance consistently.

2.3.2. ρ -start sampling

Preserving consistency with the source video is critical in video editing, particularly for maintaining structural integrity and coherent motion [37, 47, 51]. Inspired by SDEdit [24], we hypothesize that initiating the sampling process from a less perturbed latent, closer to the source video, helps retain both spatial structure and temporal dynamics.

To this end, we propose an alternative sampling strategy that modifies the standard DDIM schedule by starting the denoising process from a less noisy latent representation, thereby improving structural and temporal fidelity (Fig. 4(d)). In the conventional reduced DDIM schedule [36], sampling proceeds along a trajectory $z_{\tau_1}, \dots, z_{\tau_\nu}$, starting from a highly noisy latent z_{τ_ν} . In contrast, our approach begins from an earlier timestep, z_{τ_ρ} , where $\rho < \nu$. This shortens the denoising trajectory to only ρ steps, $\{z_{\tau_1}, \dots, z_{\tau_\rho}\}$, better preserving source content overall.

The parameter ρ controls how early the sampling begins in the reverse diffusion process. A smaller ρ initiates from a latent closer to the source video, enabling better preservation of motion patterns and spatial layout, such as object direction and position. Conversely, a larger ρ facilitates greater transformation, allowing the edited video to more closely resemble the reference image in terms of object appearance. By adjusting ρ , we gain fine-grained control over the degree of signal retention, enabling higher fidelity in both motion and overall scene consistency.

2.4. Zero image guidance

To enhance color fidelity, we present zero image guidance (Fig. 4(c)). It blends the conventional negative image embeddings [16, 28], defined by a zero vector of the same size as the CLIP image embedding, with a zero image guidance, which refers to the CLIP image embedding derived from an all-zero image. The final negative image guidance \bar{c}_{img} is computed as a weighted sum of the two, controlled by a blending factor γ :

$$\bar{c}_{\text{img}} = \gamma \cdot \text{CLIP}_{\text{img}}(\mathbf{I}_0) + (1 - \gamma) \cdot \mathbf{0}, \quad (11)$$

where $\gamma \in [0, 1]$ is a hyperparameter, $\mathbf{0} \in \mathbb{R}^d$ is a zero vector with the same size as the CLIP image embedding, $\text{CLIP}_{\text{img}}(\cdot)$

Table 1. **Quantitative comparison.** We compare VINO against four state-of-the-art models and two naive adaptations of image editing and video generation models for video editing. We measure performance using both automatic metrics and human evaluations to assess text, image, and motion alignment, temporal consistency, and overall quality.

Method	Model support			Model scoring metrics				Human evaluations				
	Text	Image	Train-free	DINO \uparrow	CLIP-T \uparrow	Temp \uparrow	PSNR \uparrow	Image \downarrow	Text \downarrow	Motion \downarrow	Temp \downarrow	Overall \downarrow
SDEdit-Video [†] [24]	✓	✗	✓	0.431	0.303	0.959	16.3	4.89	5.08	5.93	5.02	5.36
FateZero [30]	✓	✗	✓	0.438	0.311	0.967	20.1	4.59	4.53	4.44	5.06	4.75
Video-P2P [23]	✓	✗	✗	0.424	0.305	0.971	19.0	4.00	4.07	3.68	4.09	3.70
TokenFlow [11]	✓	✗	✓	<u>0.480</u>	0.325	0.975	19.6	<u>3.78</u>	<u>3.09</u>	<u>2.61</u>	<u>2.50</u>	<u>2.95</u>
AnimateDiff [13]+IPA [46]	✓	✓	✓	0.399	0.308	0.955	24.7	4.59	5.01	5.24	4.30	4.93
Make-A-Pro [50]	✓	✓	✗	0.444	0.309	0.965	16.9	3.93	4.24	3.64	5.00	4.35
VINO (Ours)	✓	✓	✓	0.498	<u>0.321</u>	<u>0.972</u>	<u>23.4</u>	2.22	1.98	2.46	2.03	1.96

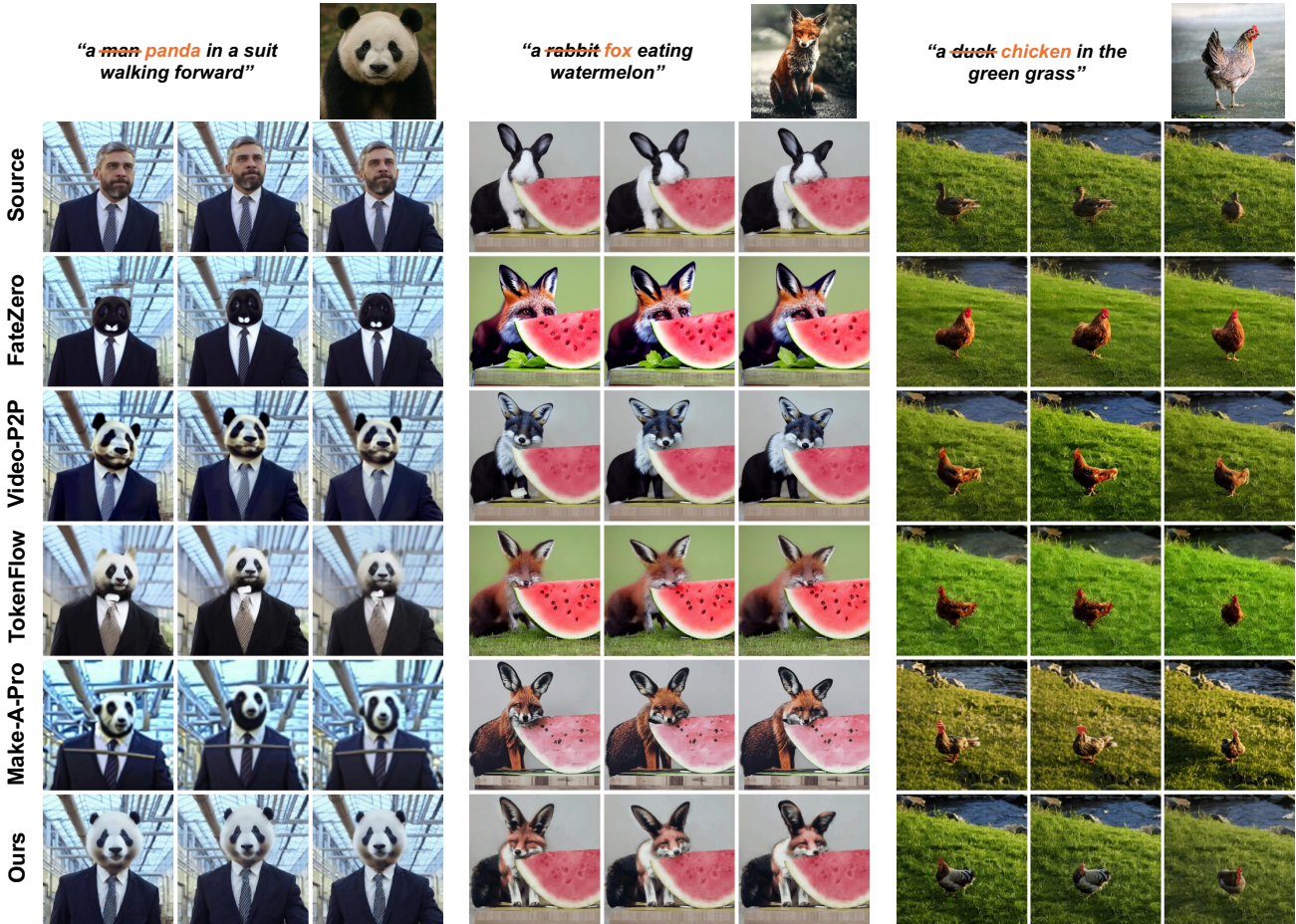


Figure 6. **Qualitative comparison.** We compare the generation quality of VINO against four state-of-the-art baseline models. VINO better preserves reference appearance across frames, while baselines struggle to retain key visual features of the target object.

is the CLIP image encoder, and $\mathbf{I}_0 \in \mathbb{R}^{C \times H \times W}$ is an all-zero image. This formulation offers a parameterized trade-off between the two types of negative guidance, allowing finer control over the color intensity of the generated object. The resulting \bar{c}_{img} , combined with the conventional \bar{c}_{txt} , is used as negative guidance during the sampling process in Eq. 6.

3. Experiments

Dataset. We evaluate VINO on 20 video-image pairs. Videos are sourced from DAVIS [29], Video-P2P [23], and a curated set covering various object categories (e.g., humans, animals, everyday items) to ensure broad semantic and visual diversity. Reference images include both real and synthetic samples

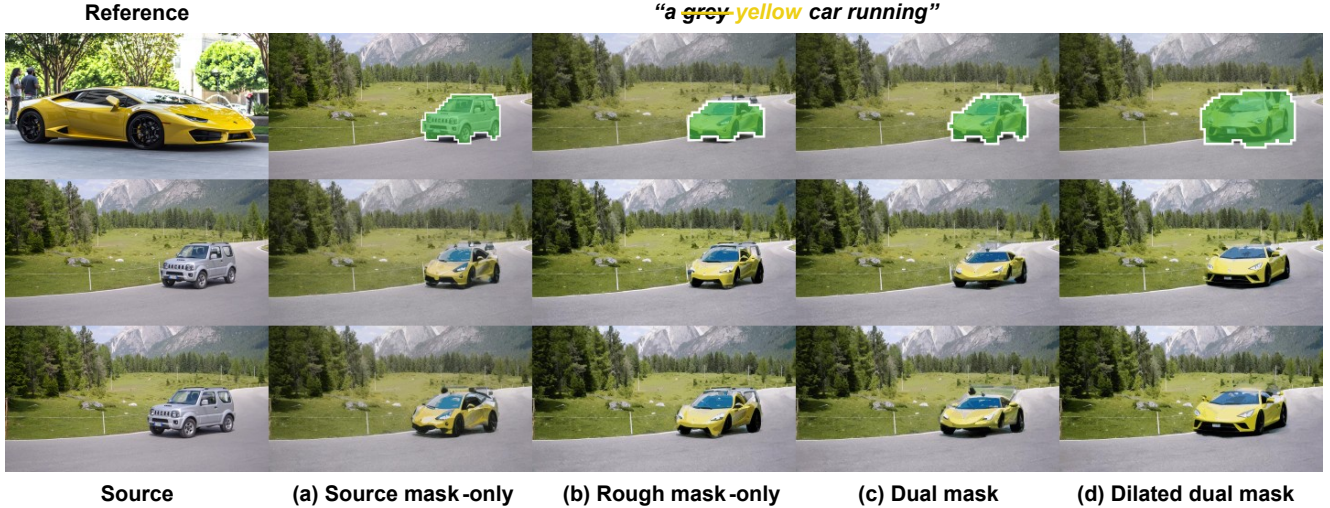


Figure 7. **Ablation study on the dilated dual masking.** The output of the first stage using the source video \mathcal{V}_s and source object mask is shown in (a). Subsequently, the outputs of the second stage from the intermediate video \mathcal{V}_r using different masking strategies are presented in (b)-(d). Masks are overlaid on the corresponding video. The proposed dilated dual masking (d) achieves the most accurate edits.

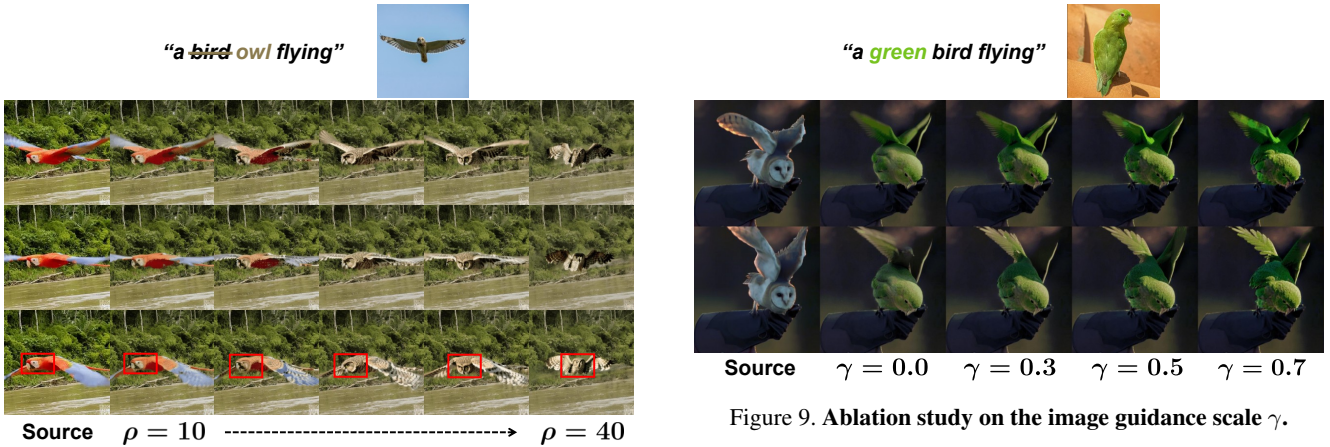


Figure 8. **Ablation study on the effect of varying the ρ value.**

generated by models such as GPT-4o and Gemini.

Baseline models. We compare VINO against six representative video editing methods, as summarized in Table 1, which use text or image prompts for semantic appearance control. SDEdit-Video[†] [24], FateZero [30], Video-P2P [23], and TokenFlow [11] represent text-guided video editing methods. To our knowledge, Make-A-Protagonist (Make-A-Pro) [50] is the only publicly available method that supports both image and text conditioning, making it the most directly comparable to VINO. AnimateDiff [13] +IP-Adapter (IPA) [46] serves as a modular baseline that integrates a pretrained T2V model with an image-guided adapter, illustrating the limitations of naive fusion strategies.

[†]We use the HuggingFace implementation of SDEdit extended to video.

Figure 9. **Ablation study on the image guidance scale γ .**

Implementation details. Our main experiments adopt AnimateDiff [13] as the base T2V model, IP-Adapter v1.5 [46] for reference image conditioning, and SAM2 [33] for mask generation. All experiments are conducted on a single NVIDIA A100 GPU. Additional implementation details, including hyperparameters, baseline setups, and extensions to other T2V backbones, are provided in Appendix E.1. Due to space constraints, we present representative qualitative comparisons and ablation results in the main paper, with full qualitative results provided in Appendix B.

3.1. Comparisons with state-of-the-art methods

Quantitative results. We evaluate VINO using four metrics: DINO score measures visual alignment via cosine similarity between features of the reference image and generated video [4]. CLIP-Text score quantifies text alignment by com-

puting cosine similarity between CLIP embeddings of the generated video and the text prompt [31]. Temporal score assesses motion consistency through cosine similarity between CLIP image embeddings of adjacent frames [31]. PSNR score measures how accurately the background of the source video is preserved by computing pixel-level similarity between the generated and source frames.

VINO achieves the highest DINO score among all baselines, indicating strong visual fidelity to the reference appearance. In CLIP-Text and temporal scores, it performs comparably to TokenFlow while outperforming other methods. Notably, VINO is compatible with existing methods such as TokenFlow and can serve as an additional appearance control module. This composition yields further performance gains, as detailed in the Appendix A. For PSNR, AnimateDiff+IPA and VINO noticeably outperform the other methods. The small gap between them, despite both using the same latent blending strategy, arises from the edited area. AnimateDiff+IPA modifies a comparatively smaller region, whereas VINO employs dilated dual masking, which introduces a larger generation area, leading to a marginally lower PSNR. **User study.** We conduct a user study with 25 participants to assess perceptual quality across five criteria: image alignment, text alignment, motion alignment, temporal consistency, and overall quality. VINO consistently outperforms all baselines across all criteria, demonstrating strong perceptual fidelity in both appearance and motion.

Qualitative results. Qualitative comparisons, shown in Fig. 6, further demonstrate the effectiveness of VINO in preserving object appearance and motion across various editing scenarios, consistently outperforming baselines.

In the man-to-panda translation, baselines either fail to generate a panda or produce artifacts or distortions, while VINO yields a clean and consistent result. A similar trend appears in the duck-to-chicken translation, where most methods generate generic chicken-like color rather than matching the reference, whereas VINO preserves its specific visual traits. In the rabbit-to-fox translation, most baselines struggle to maintain appearance fidelity or temporal coherence. Make-A-Pro, in particular, suffers from temporal flickering, including disappearing or reappearing limbs. In contrast, VINO maintains the correct fox appearance while preserving the background, producing coherent structure and stable motion throughout the video.

3.2. Ablation study

Effectiveness of dilated dual masking. We conduct an ablation study on our dilated dual masking by progressively applying different masking schemes (Fig. 7). Using only the source mask constrains the generation to the contours of the source object, often resulting in unrealistic shapes and artifacts when the source and target differ significantly (Fig. 7(a)). Applying only the rough mask alleviates

Table 2. **Comprehensive ablation study of VINO.** We evaluate the contribution of each component to the overall performance of our method: (a) base model, (b) ρ -start sampling, (c) dual masking, (d) dilation, and (e) zero image guidance.

Method	DINO \uparrow	CLIP-T \uparrow	Temp \uparrow
(a)	0.399	0.308	<u>0.955</u>
(a) + (b)	0.429	0.311	0.953
(a) + (b) + (c)	0.466	<u>0.316</u>	0.954
(a) + (b) + (c) + (d)	0.474	<u>0.316</u>	<u>0.955</u>
(a) + (b) + (c) + (d) + (e)	0.498	0.321	0.972

this issue but leaves visible remnants of the source object (Fig. 7(b)). Taking the union of both masks suppresses these remnants but introduces boundary artifacts and limits the detail due to the rigid mask constraint (Fig. 7(c)).

In contrast, our dilated dual masking effectively mitigates these limitations by dilating both masks before fusion, enabling the generated object to extend beyond the strict union region. This flexibility promotes more natural shape adaptation and smoother blending with the surrounding context (Fig. 7(d)). As a result, our dilated dual masking achieves both structural coherence and visual realism.

Effectiveness of ρ -start sampling. As shown in Fig. 8, adjusting ρ , which controls the sampling start point, enables a trade-off between target appearance and source motion. Larger ρ values cause the model to deviate from the source motion and layout. For example, the parrot facing left in the source video becomes an owl facing forward in the edited result. Smaller ρ values better preserve the source motion and spatial dynamics, producing an owl that correctly faces sideways. However, overly small ρ weakens the transformation, leading to incomplete replacement of the source object. An appropriate choice of ρ achieves a balanced edit, maintaining both appearance fidelity and motion preservation.

Effectiveness of zero image guidance. We analyze the impact of γ in our zero image guidance. As shown in Fig. 9, increasing γ , which scales the strength of the zero image guidance (see Eq. (11)), leads to more saturated colors. This suggests that incorporating the zero image guidance into the negative image effectively enhances color intensity, providing a simple yet powerful control for visual appearance.

Quantitative results. Table 2 summarizes the effect of each component in our method. As we progressively add components (a)–(e), DINO and CLIP-Text scores increase monotonically, indicating that the proposed modules jointly improve appearance transfer from the reference image as well as adherence to the text prompt. In contrast, the temporal score remains relatively stable for variants (a)–(d), but improves significantly once zero image guidance (e) is introduced, leading our complete model to achieve the best performance across all metrics. These results quantitatively demonstrate

that each component contributes effectively to temporally coherent video editing conditioned on both image and text.

4. Conclusion

In this work, we propose VINO, a novel zero-shot, training-free video editing method guided by both image and text prompts. It enables accurate object replacement with strong temporal coherence, outperforming state-of-the-art methods in visual quality and motion consistency, and efficiency.

References

- [1] Omri Avrahami, Dani Lischinski, and Ohad Fried. Blended diffusion for text-driven editing of natural images. In *Proceedings of the IEEE/CVF conference on computer vision and pattern recognition*, pages 18208–18218, 2022. 4, 5
- [2] Omri Avrahami, Ohad Fried, and Dani Lischinski. Blended latent diffusion. *ACM transactions on graphics (TOG)*, 42(4): 1–11, 2023. 4
- [3] Tim Brooks, Aleksander Holynski, and Alexei A Efros. Instructpix2pix: Learning to follow image editing instructions. In *Proceedings of the IEEE/CVF conference on computer vision and pattern recognition*, pages 18392–18402, 2023. 14
- [4] Mathilde Caron, Hugo Touvron, Ishan Misra, Hervé Jégou, Julien Mairal, Piotr Bojanowski, and Armand Joulin. Emerging properties in self-supervised vision transformers. In *Proceedings of the IEEE/CVF international conference on computer vision*, pages 9650–9660, 2021. 7
- [5] Wenhao Chai, Xun Guo, Gaoang Wang, and Yan Lu. Stablevideo: Text-driven consistency-aware diffusion video editing. In *Proceedings of the IEEE/CVF International Conference on Computer Vision*, pages 23040–23050, 2023. 1
- [6] Tsai-Shien Chen, Aliaksandr Siarohin, Willi Menapace, Yuwei Fang, Kwot Sin Lee, Ivan Skorokhodov, Kfir Aberman, Jun-Yan Zhu, Ming-Hsuan Yang, and Sergey Tulyakov. Multi-subject open-set personalization in video generation. *arXiv preprint arXiv:2501.06187*, 2025. 14
- [7] Xi Chen, Yutong Feng, Mengting Chen, Yiyang Wang, Shilong Zhang, Yu Liu, Yujun Shen, and Hengshuang Zhao. Zero-shot image editing with reference imitation. *Advances in Neural Information Processing Systems*, 37:84010–84032, 2024. 2
- [8] Paul Couairon, Clément Rambour, Jean-Emmanuel Haugeard, and Nicolas Thome. Videdit: Zero-shot and spatially aware text-driven video editing. *Transactions on Machine Learning Research*, 2023. 1
- [9] Patrick Esser, Johnathan Chiu, Parmida Atighehchian, Jonathan Granskog, and Anastasis Germanidis. Structure and content-guided video synthesis with diffusion models. In *Proceedings of the IEEE/CVF international conference on computer vision*, pages 7346–7356, 2023. 1
- [10] Shanghua Gao, Zhijie Lin, Xingyu Xie, Pan Zhou, Ming-Ming Cheng, and Shuicheng Yan. Editanything: Empowering unparalleled flexibility in image editing and generation. In *Proceedings of the 31st ACM International Conference on Multimedia*, pages 9414–9416, 2023. 14
- [11] Michal Geyer, Omer Bar-Tal, Shai Bagon, and Tali Dekel. Tokenflow: Consistent diffusion features for consistent video editing. In *The Twelfth International Conference on Learning Representations*, 2024. 1, 6, 7, 12, 17, 19, 20, 21, 22, 23
- [12] Yuchao Gu, Yipin Zhou, Bichen Wu, Licheng Yu, Jia-Wei Liu, Rui Zhao, Jay Zhangjie Wu, David Junhao Zhang, Mike Zheng Shou, and Kevin Tang. Videoswap: Customized video subject swapping with interactive semantic point correspondence. In *Proceedings of the IEEE/CVF Conference on Computer Vision and Pattern Recognition*, pages 7621–7630, 2024. 2, 4, 15
- [13] Yuwei Guo, Ceyuan Yang, Anyi Rao, Zhengyang Liang, Yao-hui Wang, Yu Qiao, Maneesh Agrawala, Dahua Lin, and Bo Dai. Animatediff: Animate your personalized text-to-image diffusion models without specific tuning. *arXiv preprint arXiv:2307.04725*, 2023. 6, 7, 12, 13, 14, 17, 19, 20, 21, 22, 23
- [14] Sai Sree Harsha, Ambareesh Revanur, Dhwanit Agarwal, and Shradha Agrawal. Genvideo: One-shot target-image and shape aware video editing using t2i diffusion models. In *Proceedings of the IEEE/CVF Conference on Computer Vision and Pattern Recognition*, pages 7559–7568, 2024. 1, 4, 15
- [15] Amir Hertz, Ron Mokady, Jay Tenenbaum, Kfir Aberman, Yael Pritch, and Daniel Cohen-Or. Prompt-to-prompt image editing with cross attention control. *arXiv preprint arXiv:2208.01626*, 2022. 14
- [16] Jonathan Ho and Tim Salimans. Classifier-free diffusion guidance. *arXiv preprint arXiv:2207.12598*, 2022. 3, 5
- [17] Wenyi Hong, Ming Ding, Wendi Zheng, Xinghan Liu, and Jie Tang. Cogvideo: Large-scale pretraining for text-to-video generation via transformers. *arXiv preprint arXiv:2205.15868*, 2022. 14
- [18] Levon Khachatryan, Andranik Movsisyan, Vahram Tadevosyan, Roberto Henschel, Zhangyang Wang, Shant Navasardyan, and Humphrey Shi. Text2video-zero: Text-to-image diffusion models are zero-shot video generators. In *Proceedings of the IEEE/CVF International Conference on Computer Vision*, pages 15954–15964, 2023. 15
- [19] Jeongho Kim, Guojung Gu, Minho Park, Sunghyun Park, and Jaegul Choo. Stableviton: Learning semantic correspondence with latent diffusion model for virtual try-on. In *Proceedings of the IEEE/CVF conference on computer vision and pattern recognition*, pages 8176–8185, 2024. 2
- [20] Junnan Li, Dongxu Li, Silvio Savarese, and Steven Hoi. Blip-2: Bootstrapping language-image pre-training with frozen image encoders and large language models. In *International conference on machine learning*, pages 19730–19742. PMLR, 2023. 17, 19, 20, 21, 22, 23
- [21] Jun Hao Liew, Hanshu Yan, Jianfeng Zhang, Zhongcong Xu, and Jiashi Feng. Magicedit: High-fidelity and temporally coherent video editing. *arXiv preprint arXiv:2308.14749*, 2023. 1
- [22] Z Lin, W Liu, C Chen, J Lu, W Hu, TJ Fu, J Allardice, Z Lai, L Song, B Zhang, et al. Stiv: Scalable text and image conditioned video generation. *arxiv*, 2024. 14
- [23] Shaoteng Liu, Yuechen Zhang, Wenbo Li, Zhe Lin, and Jiaya

- Jia. Video-p2p: Video editing with cross-attention control, 2023. 1, 6, 7, 15, 17, 19, 20, 21, 22, 23
- [24] Chenlin Meng, Yutong He, Yang Song, Jiaming Song, Jiajun Wu, Jun-Yan Zhu, and Stefano Ermon. Sdedit: Guided image synthesis and editing with stochastic differential equations. *arXiv preprint arXiv:2108.01073*, 2021. 2, 5, 6, 7, 12, 13, 17, 19, 20, 21, 22, 23
- [25] Eyal Molad, Eliahu Horwitz, Dani Valevski, Alex Rav Acha, Yossi Matias, Yael Pritch, Yaniv Leviathan, and Yedid Hoshen. Dreamix: Video diffusion models are general video editors. *arXiv preprint arXiv:2302.01329*, 2023. 1
- [26] Chong Mou, Mingdeng Cao, Xintao Wang, Zhaoyang Zhang, Ying Shan, and Jian Zhang. Revideo: Remake a video with motion and content control. *Advances in Neural Information Processing Systems*, 37:18481–18505, 2024. 1
- [27] Haomiao Ni, Bernhard Egger, Suhas Lohit, Anoop Cherian, Ye Wang, Toshiaki Koike-Akino, Sharon X Huang, and Tim K Marks. T2v-zero: Zero-shot image conditioning for text-to-video diffusion models. In *Proceedings of the IEEE/CVF Conference on Computer Vision and Pattern Recognition*, pages 9015–9025, 2024. 14
- [28] Alex Nichol, Prafulla Dhariwal, Aditya Ramesh, Pranav Shyam, Pamela Mishkin, Bob McGrew, Ilya Sutskever, and Mark Chen. Glide: Towards photorealistic image generation and editing with text-guided diffusion models. *arXiv preprint arXiv:2112.10741*, 2021. 5
- [29] Federico Perazzi, Jordi Pont-Tuset, Brian McWilliams, Luc Van Gool, Markus Gross, and Alexander Sorkine-Hornung. A benchmark dataset and evaluation methodology for video object segmentation. In *Proceedings of the IEEE conference on computer vision and pattern recognition*, pages 724–732, 2016. 6
- [30] Chenyang Qi, Xiaodong Cun, Yong Zhang, Chenyang Lei, Xintao Wang, Ying Shan, and Qifeng Chen. Fatezero: Fusing attentions for zero-shot text-based video editing. In *Proceedings of the IEEE/CVF International Conference on Computer Vision*, pages 15932–15942, 2023. 1, 6, 7, 17, 19, 20, 21, 22, 23
- [31] Alec Radford, Jong Wook Kim, Chris Hallacy, Aditya Ramesh, Gabriel Goh, Sandhini Agarwal, Girish Sastry, Amanda Askell, Pamela Mishkin, Jack Clark, et al. Learning transferable visual models from natural language supervision. In *International conference on machine learning*, pages 8748–8763. PmLR, 2021. 4, 8
- [32] Aditya Ramesh, Prafulla Dhariwal, Alex Nichol, Casey Chu, and Mark Chen. Hierarchical text-conditional image generation with clip latents. *arXiv preprint arXiv:2204.06125*, 1(2): 3, 2022. 13
- [33] Nikhila Ravi, Valentin Gabeur, Yuan-Ting Hu, Ronghang Hu, Chaitanya Ryal, Tengyu Ma, Haitham Khedr, Roman Rädle, Chloe Rolland, Laura Gustafson, et al. Sam 2: Segment anything in images and videos. *arXiv preprint arXiv:2408.00714*, 2024. 7
- [34] Robin Rombach, Andreas Blattmann, Dominik Lorenz, Patrick Esser, and Björn Ommer. High-resolution image synthesis with latent diffusion models. In *Proceedings of the IEEE/CVF conference on computer vision and pattern recognition*, pages 10684–10695, 2022. 3, 13, 14
- [35] Chitwan Saharia, William Chan, Saurabh Saxena, Lala Li, Jay Whang, Emily L Denton, Kamyar Ghasemipour, Raphael Gontijo Lopes, Burcu Karagol Ayan, Tim Salimans, et al. Photorealistic text-to-image diffusion models with deep language understanding. *Advances in neural information processing systems*, 35:36479–36494, 2022. 13
- [36] Jiaming Song, Chenlin Meng, and Stefano Ermon. Denoising diffusion implicit models. *arXiv preprint arXiv:2010.02502*, 2020. 3, 5
- [37] Yeji Song, Wonsik Shin, Junsoo Lee, Jeeseo Kim, and Nojun Kwak. Save: Protagonist diversification with structure agnostic video editing. In *European Conference on Computer Vision*, pages 41–57. Springer, 2024. 1, 5
- [38] Spencer Sterling. zeroscope-v2. https://huggingface.co/cerspense/zeroscope_v2_576w, 2023. 14
- [39] Yuanpeng Tu, Hao Luo, Xi Chen, Sihui Ji, Xiang Bai, and Hengshuang Zhao. Videoanydoor: High-fidelity video object insertion with precise motion control. *arXiv preprint arXiv:2501.01427*, 2025. 2
- [40] Jiuniu Wang, Hangjie Yuan, Dayou Chen, Yingya Zhang, Xiang Wang, and Shiwei Zhang. Modelscope text-to-video technical report. *arXiv preprint arXiv:2308.06571*, 2023. 14
- [41] Yujie Wei, Shiwei Zhang, Zhiwu Qing, Hangjie Yuan, Zhiheng Liu, Yu Liu, Yingya Zhang, Jingren Zhou, and Hongming Shan. Dreamvideo: Composing your dream videos with customized subject and motion. In *Proceedings of the IEEE/CVF Conference on Computer Vision and Pattern Recognition*, pages 6537–6549, 2024. 14
- [42] Jay Zhangjie Wu, Yixiao Ge, Xintao Wang, Stan Weixian Lei, Yuchao Gu, Yufei Shi, Wynne Hsu, Ying Shan, Xiaohu Qie, and Mike Zheng Shou. Tune-a-video: One-shot tuning of image diffusion models for text-to-video generation. In *Proceedings of the IEEE/CVF International Conference on Computer Vision*, pages 7623–7633, 2023. 1, 15
- [43] Tao Wu, Yong Zhang, Xintao Wang, Xianpan Zhou, Guangcong Zheng, Zhongang Qi, Ying Shan, and Xi Li. Customcrafter: Customized video generation with preserving motion and concept composition abilities. *arXiv preprint arXiv:2408.13239*, 2024. 14
- [44] Binxin Yang, Shuyang Gu, Bo Zhang, Ting Zhang, Xuejin Chen, Xiaoyan Sun, Dong Chen, and Fang Wen. Paint by example: Exemplar-based image editing with diffusion models. In *Proceedings of the IEEE/CVF conference on computer vision and pattern recognition*, pages 18381–18391, 2023. 2
- [45] Shuai Yang, Yifan Zhou, Ziwei Liu, and Chen Change Loy. Rerender a video: Zero-shot text-guided video-to-video translation. In *SIGGRAPH Asia 2023 Conference Papers*, pages 1–11, 2023. 1
- [46] Hu Ye, Jun Zhang, Sibio Liu, Xiao Han, and Wei Yang. Ip-adapter: Text compatible image prompt adapter for text-to-image diffusion models. *arXiv preprint arXiv:2308.06721*, 2023. 2, 4, 6, 7, 12, 13, 14, 17, 19, 20, 21, 22, 23
- [47] Guiwei Zhang, Tianyu Zhang, Guanglin Niu, Zichang Tan, Yalong Bai, and Qing Yang. Camel: Causal motion enhancement tailored for lifting text-driven video editing. In *Proceedings of the IEEE/CVF Conference on Computer Vision and Pattern Recognition*, pages 9079–9088, 2024. 5

- [48] Lvmin Zhang, Anyi Rao, and Maneesh Agrawala. Adding conditional control to text-to-image diffusion models. In *Proceedings of the IEEE/CVF international conference on computer vision*, pages 3836–3847, 2023. [14](#)
- [49] Yabo Zhang, Yuxiang Wei, Dongsheng Jiang, Xiaopeng Zhang, Wangmeng Zuo, and Qi Tian. Controlvideo: Training-free controllable text-to-video generation. *arXiv preprint arXiv:2305.13077*, 2023. [1](#), [14](#)
- [50] Yuyang Zhao, Enze Xie, Lanqing Hong, Zhenguo Li, and Gim Hee Lee. Make-a-protagonist: Generic video editing with an ensemble of experts. *arXiv preprint arXiv:2305.08850*, 2023. [1](#), [2](#), [6](#), [7](#), [15](#), [17](#), [19](#), [20](#), [21](#), [22](#), [23](#)
- [51] Xiaojing Zhong, Xinyi Huang, Xiaofeng Yang, Guosheng Lin, and Qingyao Wu. Deco: Decoupled human-centered diffusion video editing with motion consistency. In *European Conference on Computer Vision*, pages 352–370. Springer, 2024. [5](#)
- [52] Zhichao Zuo, Zhao Zhang, Yan Luo, Yang Zhao, Haijun Zhang, Yi Yang, and Meng Wang. Cut-and-paste: Subject-driven video editing with attention control. *Neural Networks*, 181:106818, 2025. [1](#), [15](#)

Appendix

This supplementary material complements the main manuscript, providing additional experimental results and implementation details that could not be included because of space limitations.

- **Appendix A** illustrates the applicability of our method across various text-to-video models.
- **Appendix B** includes complete qualitative comparison and ablation studies.
- **Appendix C** provides related work.
- **Appendix D** discusses the limitations of our method.
- **Appendix E** details additional experimental settings.
- **Appendix F** presents the overall algorithm of our method.
- **Appendix G** showcases additional qualitative results.

A. Applicability to various T2V models

As shown in Table 3, our method is compatible with various text-to-video (T2V) models, enabling training-free video editing conditioned on both images and text. We evaluate the compatibility of our approach by extending the text-based generative model AnimateDiff [13] and the text-based editing model TokenFlow [11] with our proposed components, including dilated dual masking, ρ -start sampling, zero-image guidance, and the image-guided module.

Integrating our method into AnimateDiff yields higher scores across most metrics, demonstrating substantial improvements in structural consistency and visual similarity to the reference image. When applied to TokenFlow, DINO and PSNR also improve, indicating the integration strengthens reference alignment even in the text-based editing models.

However, our method shows a lower temporal consistency score than that of text-prompt-only baselines. This reflects a trade-off inherent to image-based conditioning, where aligning each frame to a high-fidelity reference image introduces larger pixel-level variations, even though the edits remain perceptually coherent. Despite this trade-off, the consistent gains achieved with only marginal drops in temporal consistency across both generation and editing models underscore the applicability and generality of our method.

B. Full qualitative comparison and ablations

This section presents the full qualitative comparisons with baseline methods and qualitative ablation results that complement those in the main paper. Appendix B.1 includes complete qualitative comparison against baseline approaches, Appendix B.2 provides full results for ablation studies.

B.1. Qualitative comparison with baselines

As shown in Fig. 10, since SDEdit-Video [24] and AnimateDiff [13]+IP-Adapter [46] are adapted or composed from methods not originally designed for video editing, their

Table 3. **Quantitative evaluation of applicability to various T2V models.** We integrate our proposed components into AnimateDiff and TokenFlow. The integration improves reference alignment and image quality with minimal trade-offs across different architectures.

Method	Model scoring metrics			
	DINO \uparrow	CLIP-T \uparrow	Temp \uparrow	PSNR \uparrow
AnimateDiff [13]	0.412	0.308	0.980	13.9
+ Ours	0.498	0.321	0.972	24.7
TokenFlow [11]	0.480	0.325	0.975	19.6
+ Ours	0.523	0.320	0.974	23.9

qualitative results exhibit reduced visual fidelity compared to other baseline methods. Specifically, SDEdit-Video is extended from its original image-based formulation to the video domain, while AnimateDiff+IP-Adapter combines AnimateDiff with IP-Adapter in a naive manner. As a result, SDEdit-Video preserves only the coarse spatial layout of the source video and often introduces excessive noise, leading to degraded visual quality. In the case of AnimateDiff+IP-Adapter, reference images are directly pasted into the edited regions without sufficient consideration of semantic structure, resulting in visually unnatural artifacts.

B.2. Qualitative ablation studies

Dilated dual masking. Dilated dual masking enables the seamless replacement of the source object with the target object in the reference image across frames. Fig. 11 presents the complete results of Fig. 7, confirming that the patterns observed remain consistent across different frames.

In Fig. 11(a), when only the source mask is used, the target object is unnaturally constrained to the shape of the source mask, resulting in distortion. In Fig. 11(b), using only the rough mask fails to fully cover the source object, leaving undesired remnants of it in the edited video. In Fig. 11(c), employing a dual mask obtained by taking the union of the source and target masks, alleviates artifacts from the source object and shape mismatches of the target object, but the mask boundaries still lack smoothness. In contrast, our dilated dual mask in Fig. 11(d) effectively mitigates these, enabling clean removal of the source object and coherent synthesis of the target object throughout the video.

ρ -start sampling. Our ρ -start sampling initiates DDIM sampling and inversion from intermediate time steps, thereby balancing the appearance of the reference image with the spatial layout of the source video. Fig. 12 supplements Fig. 8 by additionally presenting the final edited video results. Specifically, while Fig. 8 only illustrates the first stage edits under varying values of ρ , the rightmost column in Fig. 12 provides the corresponding final outputs after the second stage. The second stage further refines facial details, producing results that more closely resemble the reference image.

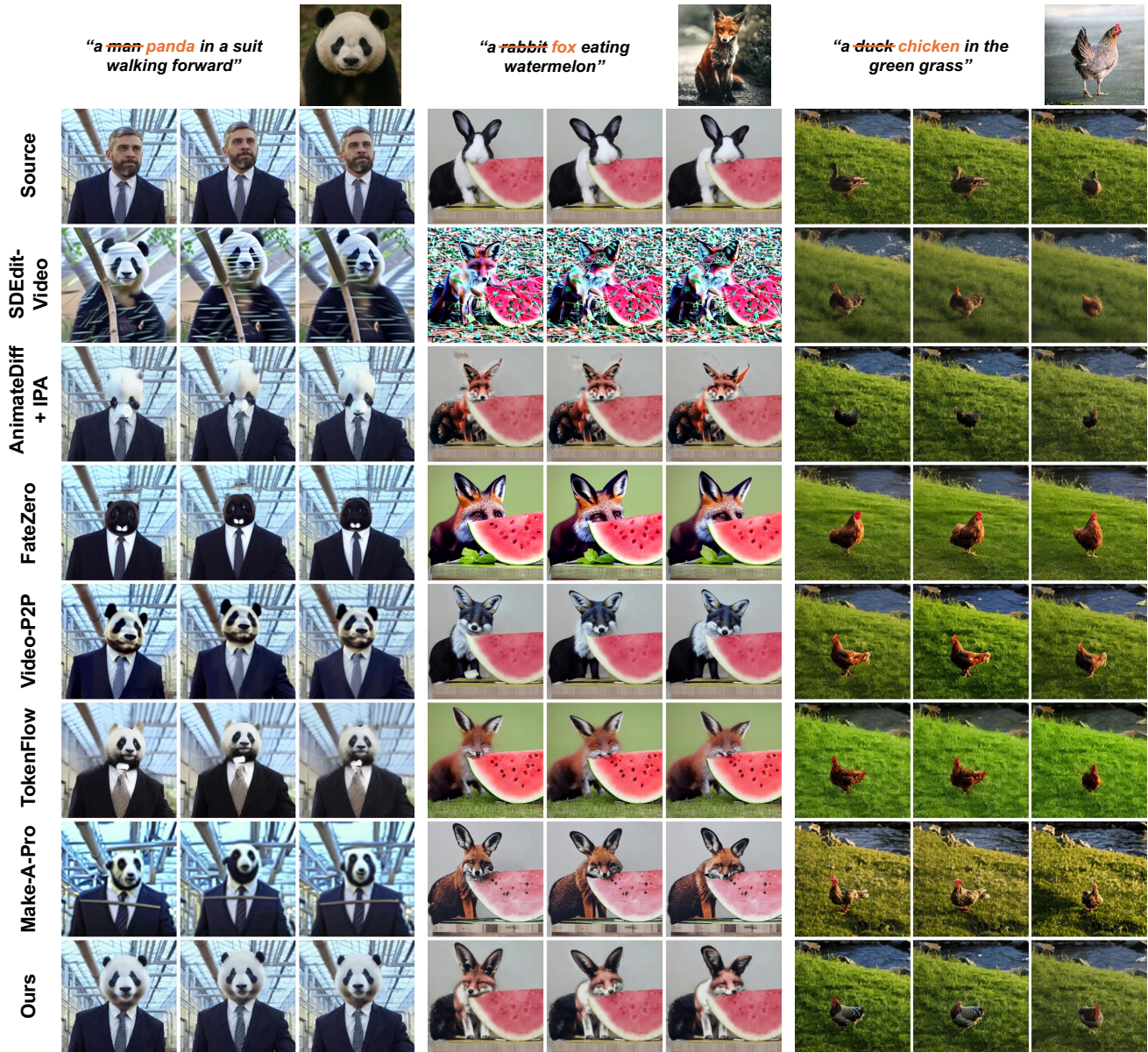


Figure 10. **Full qualitative comparison with baselines.** We provide an extended version of Fig. 6 from the main manuscript by including results from SDEdit-Video [24] and AnimateDiff [13]+IP-Adapter [46].

Zero image guidance. Zero image guidance is introduced specifically to handle the occasional color desaturation observed in the edited videos. By adjusting the negative prompt to steer the generation away from the zero image direction, this mechanism effectively enhances color fidelity. Figure 13 provides an extension of the results in Figure 9 by presenting edits across a wider range of γ values. As γ approaches 1, the contribution of zero image guidance within the negative image guidance increases, leading to noticeably improved color saturation in the edited videos.

C. Related work

C.1. Image and video generation

Recent advancements in latent diffusion models (LDMs) have significantly improved the fidelity and controllability of image generation. Text-to-image (T2I) models such as Stable Diffusion [34], DALL-E 2 [32], and Imagen [35] achieve high-resolution image synthesis aligned with complex text prompts. These models operate in the latent space for computational efficiency and support diverse conditioning mech-

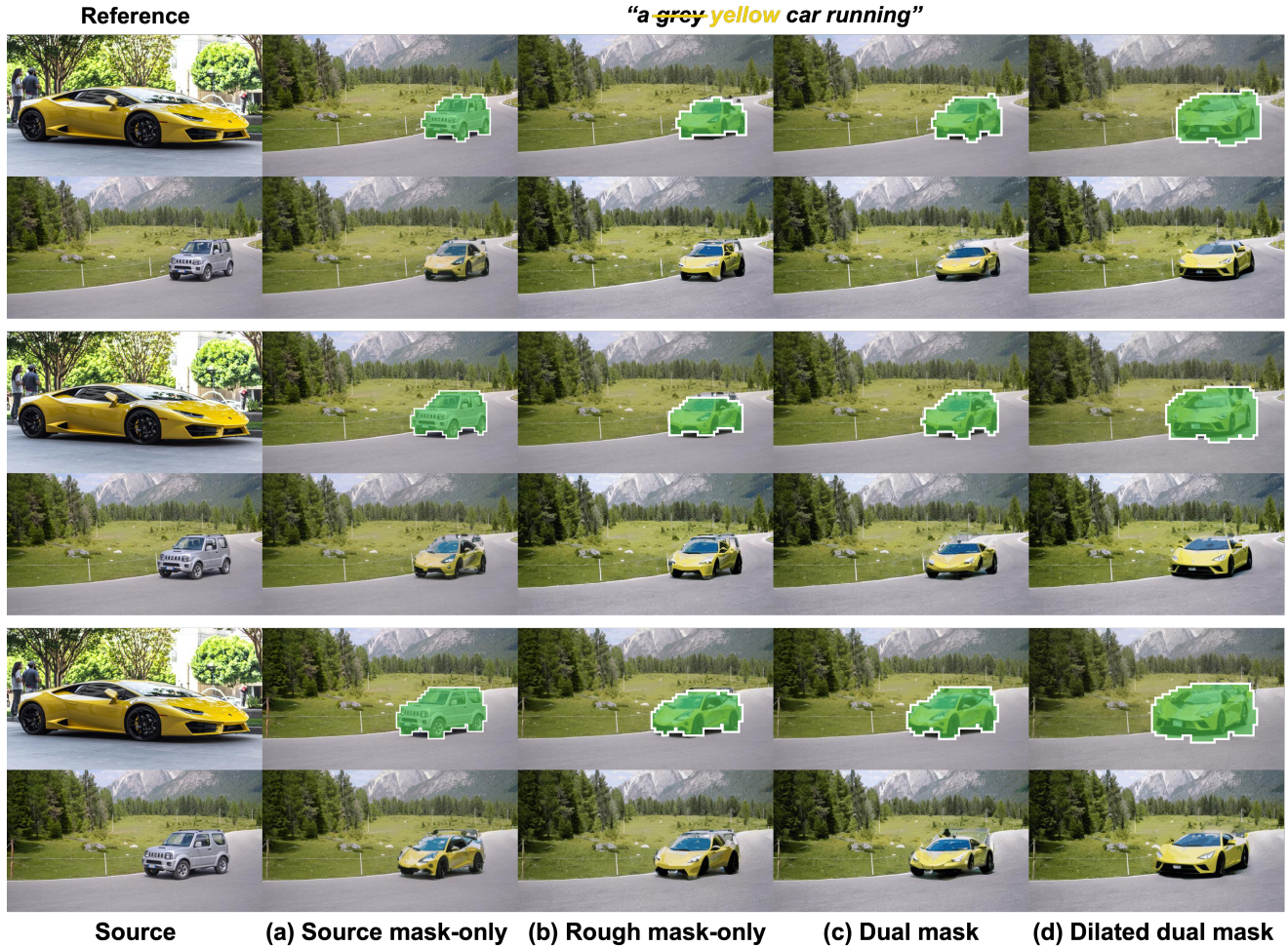


Figure 11. **Full qualitative results of the ablation study on dilated dual masking.** Additional frames corresponding to Fig. 7 in the main manuscript are provided to further illustrate the consistent transformation of the object across time.

anisms, including text, layout, and edge maps [46, 48]. Their flexibility has made LDMs foundational components for extending generative modeling into the video domain.

Motivated by T2I success, text-to-video (T2V) models have emerged to generate coherent video sequences conditioned on textual descriptions. CogVideo [17] adapts T2I backbones with temporal attention, enabling efficient video generation with minimal overhead. ZeroScope [38], built on ModelScope [40], improves visual fidelity and consistency, producing higher-resolution outputs while mitigating common artifacts in earlier methods. AnimateDiff [13] integrates temporal modules into Stable Diffusion [34], facilitating the T2V model with improved coherence between frames.

Alongside architectural advances, controllability and identity preservation have gained importance. Several methods leverage a reference frame along with a prompt to guide spatial appearance and layout across time [22, 27, 49]. In addition, others introduce subject-driven personalization via in-

stance finetuning [6, 41–43], enabling video generation with identity consistency across diverse prompts. These trends illustrate a broader shift toward multimodal conditioning across text, image, and motion to allow more expressive and controllable video synthesis.

C.2. Image and video editing

Following the advances in image and video generation models, diffusion models have also made significant progress in image and video editing, allowing precise content manipulation. In the image domain, Prompt-to-Prompt [15] introduces cross-attention manipulation within pretrained diffusion models, enabling semantic edits without finetuning or masks. InstructPix2Pix [3] leverages pairs of instructions and images to support editing guided by natural language. EditAnything [10] generalizes this paradigm by integrating multi-modal inputs such as text, masks, and user clicks.

Video editing extends these capabilities to the temporal



Figure 12. **Full qualitative results of the ablation study on the ρ -start sampling.** We present the complete results corresponding to Fig. 8 in the main manuscript by adding final edited results. As the value of ρ increases from 10 to 40 in Stage 1, the parrot in the source video gradually transforms to more closely resemble the owl in the reference image. After processing through Stage 2, the final edits further align with the reference appearance and exhibit improved visual quality.

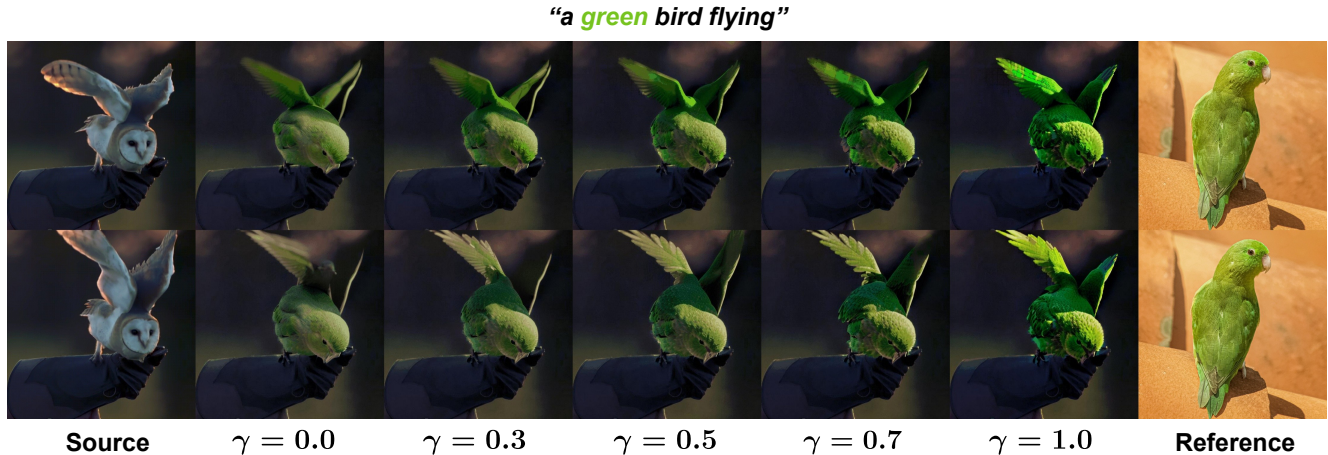


Figure 13. **Full qualitative results of the ablation study on the zero image guidance scale γ .** We include the complete results corresponding to Fig. 9 in the main paper. As the γ value is adjusted, the color fidelity of the edited video is calibrated to better match the reference image.

dimension. Tune-A-Video [42] employs one-shot tuning of pretrained image diffusion models for video editing tasks, allowing users to modify video content and style with minimal data and strong temporal consistency. Video-P2P [23] extends cross-attention control techniques from image to video, maintaining both spatial and temporal coherence. Text2Video-Zero [18] removes the need for paired text-video data, instead leveraging pretrained text-image models for flexible and data-efficient video editing.

To overcome the limitations of editing based solely on text, recent studies propose image-conditioned video editing

methods that use a reference image to guide appearance and identity [14, 50, 52]. Make-A-Protagonist [50] introduces a unified framework for protagonist replacement, background editing, and style transfer using mask-guided denoising. Gen-Video [14] proposes shape-aware masking and latent noise correction to ensure temporal consistency and subject fidelity. VideoSwap [12] adds semantic point correspondences to provide interactive and precise control over the subject’s motion and appearance. Despite these advancements, existing methods still require finetuning on each source video and rely on user-defined semantic keypoints, limiting practicality and



Figure 14. **Example of failure case.** A large semantic gap between the object in the source video and the reference image poses challenges for our method. We show results from two versions of our method, obtained by varying the sampling start point ρ and the dilation kernel size. In this case, editing a bird into a red panda results in missing or incorrect transfer of the wings and arms.

scalability. In contrast, our method directly utilizes the image prompt without any finetuning, while effectively preserving temporal consistency and semantic accuracy.

D. Limitation

Although our method exhibits notable improvements over existing baselines, as evidenced by extensive experiments, it still faces certain limitations. When there is a substantial disparity in the innate physical characteristics between the source and target objects, our method struggles to perform object replacement. Figure 14 shows that our method generates wings for the red panda which is an anatomically implausible feature to transfer the parrot’s flying motion. Conversely, in attempting to preserve the red panda’s natural characteristics, it fails to convey the intended motion.

E. Additional experimental settings

Appendix E.1 provides further implementation details, including hyperparameter settings. Appendix E.2 outlines the reproducibility settings for all baseline models used in our experiments. Appendix E.3 presents the evaluation questions used in our user study.

E.1. Additional implementation details

Our method introduces four key hyperparameters: ρ , γ , dilation kernel size, and guidance scale. Each parameter has a well-defined and narrow range that yields consistent per-

formance across diverse editing tasks. Consequently, hyperparameter tuning in the proposed method requires minimal manual adjustment and can be efficiently performed without extensive search or optimization.

- $\rho \in [10, 30]$: Controls the starting timestep for the denoising trajectory. In practice, one of the discrete values (10, 20, or 30) generally performs well. Users may optionally refine the result by exploring intermediate values.
- $\gamma \in [0, 1]$: Controls the weighted combination of standard zero-vector and zero-image embeddings in zero image guidance. The default value of 0.5 has been empirically found to perform robustly across a wide variety of scenes, object types, and motion dynamics.
- dilation kernel size $k \in [0, 10]$: Defines the kernel size used in the dilated dual masking. It affects the spatial smoothness and coverage of the edited region. The default value of 3 works well in most cases, while slightly larger values (e.g., 5 or 7) can help when the source and target objects differ significantly in shape or size.
- guidance scale $\in [6, 10]$: Determines the strength of classifier-free guidance during denoising. The default setting of 6 typically yields semantically faithful results.

Depending on the resolution of the source video, we use one of the following sizes: 320×576, 432×768, 480×480, 515×512, 600×600, 640×640, or 700×700. As an exception, the results in Fig. 1 are rendered at 1024×576 to better showcase our method’s performance. The number of frames is set to 8 or 16, selected according to the source video length.

E.2. Reproducibility of baseline models

All baseline models are run using the official implementations released in their GitHub repositories. For a fair comparison, we evaluate all baselines under the same experimental settings as our method unless specified otherwise (refer to Appendix E.1). The same text prompts are applied across all methods, except for the method that follows its own text prompting strategy. We also use the same spatial resolution for VINO and all baseline models, except for methods that inherently require square inputs.

- **SDEdit-Video** [24]¹ We adopt the video-extended implementation provided by HuggingFace, as the original SDEdit is originally image-based.
- **FateZero** [30]² As FateZero [30] supports only square outputs, we paste its generated video into the corresponding region of the source video for comparison. Both FateZero [30] and Make-A-Pro [50] employ model-based prompting procedures to automatically generate text prompts. While FateZero originally uses an earlier BLIP variant for this step, the overall prompting procedure is fundamentally the same as that of Make-A-Protagonist, which uses BLIP-2. To maintain consistency, we adopt the more recent BLIP-2–based prompting strategy for FateZero as well and use identical text prompts for both methods.
- **Video-P2P** [23]³ Similar to FateZero, since Video-P2P [23] produces square outputs, we paste its generated video into the corresponding region of the source video.
- **TokenFlow** [11]⁴ TokenFlow is evaluated under the same experimental settings as our method without any additional modifications. To implement **TokenFlow+Ours**, we extend TokenFlow by adding IP-Adapter [46] to support image conditioning, and incorporate our proposed approaches, including zero-image guidance, ρ -start sampling, and dilated dual masking.
- **AnimateDiff** [13]⁵+**IP-Adapter** [46]⁶ For both AnimateDiff and IP-Adapter, we use their official GitHub implementations, and fuse the two following the integration scheme proposed in the IP-Adapter paper.
- **Make-A-Protagonist** [50]⁷ Following the original prompt generation strategy, we extract protagonist cues using BLIP-2 [20] and generate prompts via visual question answering as provided in its official GitHub repository.

¹https://github.com/huggingface/diffusers/blob/main/src/diffusers/pipelines/animatediff/pipeline_animatediff_video2video.py

²<https://github.com/ChenyangQiQi/FateZero>

³<https://github.com/dvlab-research/Video-P2P>

⁴<https://github.com/omerbt/TokenFlow>

⁵<https://github.com/guoyww/AnimateDiff>

⁶<https://github.com/tencent-ailab/IP-Adapter>

⁷<https://github.com/HeliosZhao/Make-A-Protagonist>

E.3. User study details

In the user study described in Section 3.1, participants were asked to rank the seven generated videos from 1st (best) to 7th (worst) for each of the following five evaluation criteria:

- **Image Alignment:** How well the appearance of the "object in the generated video" matches the "object in the reference image (excluding the background)".
- **Text Alignment:** How well "the content of the generated video" aligns with the "provided text prompt".
Text prompt: "a polar bear skiing"
- **Motion Alignment:** How closely the "motion of the object in the generated video" matches the "motion of the object in the source video".
- **Temporal Consistency:** The degree to which the object and background remain consistent across time.
- **Overall Quality:** The overall realism and naturalness of the edited video, considering all aspects above.

F. Algorithm

The overall video editing pipeline of VINO is outlined in Algorithm 1. Our training-free method consists of two stages: a rough editing stage that generates an initial object transformation guided by the source mask, and a refinement stage that further improves visual fidelity and temporal coherence using an updated mask derived from the intermediate result.

G. Additional qualitative results

Additional qualitative comparisons with baseline methods are provided in Fig. 15, Fig. 16, Fig. 17, Fig. 18, and Fig. 19, which further demonstrate the superior visual fidelity and temporal consistency achieved by our approach. Notably, AnimateDiff+IP-Adapter frequently exhibits noticeable distortions in both shape and color, leading to unnatural visual artifacts. To address this, our method constructs a well-formed noise maps by selecting a less-degraded latent via ρ -start sampling and combining foreground and background latents through dilated dual masking. This structured noise formulation enables accurate object replacement while preserving the motion dynamics of the source video.

Algorithm 1 Training-free video editing procedure of VINO

Input: Source video \mathcal{V}_s , image prompt \mathcal{R} , text prompt \mathcal{T} , negative text prompt $\bar{\mathcal{T}}$

Output: Edited video \mathcal{V}_e

Prompt feature extraction

- 1: $\mathbf{c}_{\text{img}} \leftarrow \text{CLIP}_{\text{img}}(\mathcal{R}), \mathbf{c}_{\text{txt}} \leftarrow \text{CLIP}_{\text{txt}}(\mathcal{T})$
- 2: $\bar{\mathbf{c}}_{\text{img}} = \gamma \cdot \text{CLIP}_{\text{img}}(\mathbf{I}_0) + (1 - \gamma) \cdot \mathbf{0}, \bar{\mathbf{c}}_{\text{txt}} = \gamma \cdot \text{CLIP}_{\text{txt}}(\bar{\mathcal{T}})$, where $\gamma \in [0, 1]$

Stage 1: Rough editing

Dilated mask generation

- 3: $M_s \leftarrow \text{Segment}(\mathcal{V}_s)$
- 4: $M'_s \leftarrow \text{Dilate}(M_s)$

Latent encoding

- 5: $\mathbf{z}_0 \leftarrow \mathcal{E}(\mathcal{V}_s)$
- 6: $\{\mathbf{z}_t\}_{t=\tau_1}^{\tau_\nu} \leftarrow \text{DDIM-inv}(\mathbf{z}_0)$

Denoising

- 7: Select $\rho \in [\nu]$
- 8: $\mathbf{z}'_{\tau_\rho} \leftarrow \sqrt{\alpha_{\tau_\rho}} \cdot \mathbf{z}_0 + \sqrt{1 - \alpha_{\tau_\rho}} \cdot \eta$, where $\eta \sim \mathcal{N}(0, \mathbf{I})$
- 9: **for** $t = \rho$ to 1 **do**
- 10: $\mathbf{z}'_{\tau_{t-1}} \leftarrow \text{DDIM-samp}(\mathbf{z}'_{\tau_t}, \mathbf{c}_{\text{img}}, \mathbf{c}_{\text{txt}}, \bar{\mathbf{c}}_{\text{img}}, \bar{\mathbf{c}}_{\text{txt}}, \tau_t)$
- 11: $\mathbf{z}^{\text{bg}}_{\tau_{t-1}} \leftarrow \mathbf{z}_{\tau_{t-1}}$
- 12: $\mathbf{z}'_{\tau_{t-1}} \leftarrow \mathbf{z}'_{\tau_{t-1}} \odot M'_s + \mathbf{z}^{\text{bg}}_{\tau_{t-1}} \odot (1 - M'_s)$
- 13: **end for**

Latent decoding

- 14: $\mathcal{V}_r \leftarrow \mathcal{D}(\mathbf{z}'_{\tau_0})$
- 15: $\mathcal{V}_r \leftarrow \mathcal{V}_r \odot M'_s + \mathcal{V}_s \odot (1 - M'_s)$

Stage 2: Refined editing

Dilated dual mask generation

- 16: $M_r \leftarrow \text{Segment}(\mathcal{V}_r)$
- 17: $M'_r \leftarrow \text{Dilate}(M_r)$
- 18: $M_e \leftarrow M'_s \cup M'_r$

Latent encoding

- 19: $\mathbf{z}_0 \leftarrow \mathcal{E}(\mathcal{V}_r)$
- 20: $\{\mathbf{z}_t\}_{t=\tau_1}^{\tau_\nu} \leftarrow \text{DDIM-inv}(\mathcal{E}(\mathcal{V}_s))$

Denoising

- 21: Select $\rho \in [\nu]$
- 22: $\mathbf{z}'_{\tau_\rho} \leftarrow \sqrt{\alpha_{\tau_\rho}} \cdot \mathbf{z}_0 + \sqrt{1 - \alpha_{\tau_\rho}} \cdot \eta$, where $\eta \sim \mathcal{N}(0, \mathbf{I})$
- 23: **for** $t = \rho$ to 1 **do**
- 24: $\mathbf{z}'_{\tau_{t-1}} \leftarrow \text{DDIM-samp}(\mathbf{z}'_{\tau_t}, \mathbf{c}_{\text{img}}, \mathbf{c}_{\text{txt}}, \bar{\mathbf{c}}_{\text{img}}, \bar{\mathbf{c}}_{\text{txt}}, \tau_t)$
- 25: $\mathbf{z}^{\text{bg}}_{\tau_{t-1}} \leftarrow \mathbf{z}_{\tau_{t-1}}$
- 26: $\mathbf{z}'_{\tau_{t-1}} \leftarrow \mathbf{z}'_{\tau_{t-1}} \odot M_e + \mathbf{z}^{\text{bg}}_{\tau_{t-1}} \odot (1 - M_e)$
- 27: **end for**

Latent decoding

- 28: $\mathcal{V}_e \leftarrow \mathcal{D}(\mathbf{z}'_{\tau_0})$
-

"a **white** duck in the water"



Figure 15. **Complete video editing comparisons with baseline methods.** FateZero [30] and Make-a-Pro [50] use text prompts generated by BLIP-2 [20], following their respective proposed strategies. TokenFlow [11], Video-P2P [23], FateZero [30], and SDEdit-Video [24] use only text prompts, while Make-a-Pro [50], AnimateDiff [13]+IP-Adapter [46], and our proposed method use both image and text prompts.

“a *child* *red panda* riding a bike”

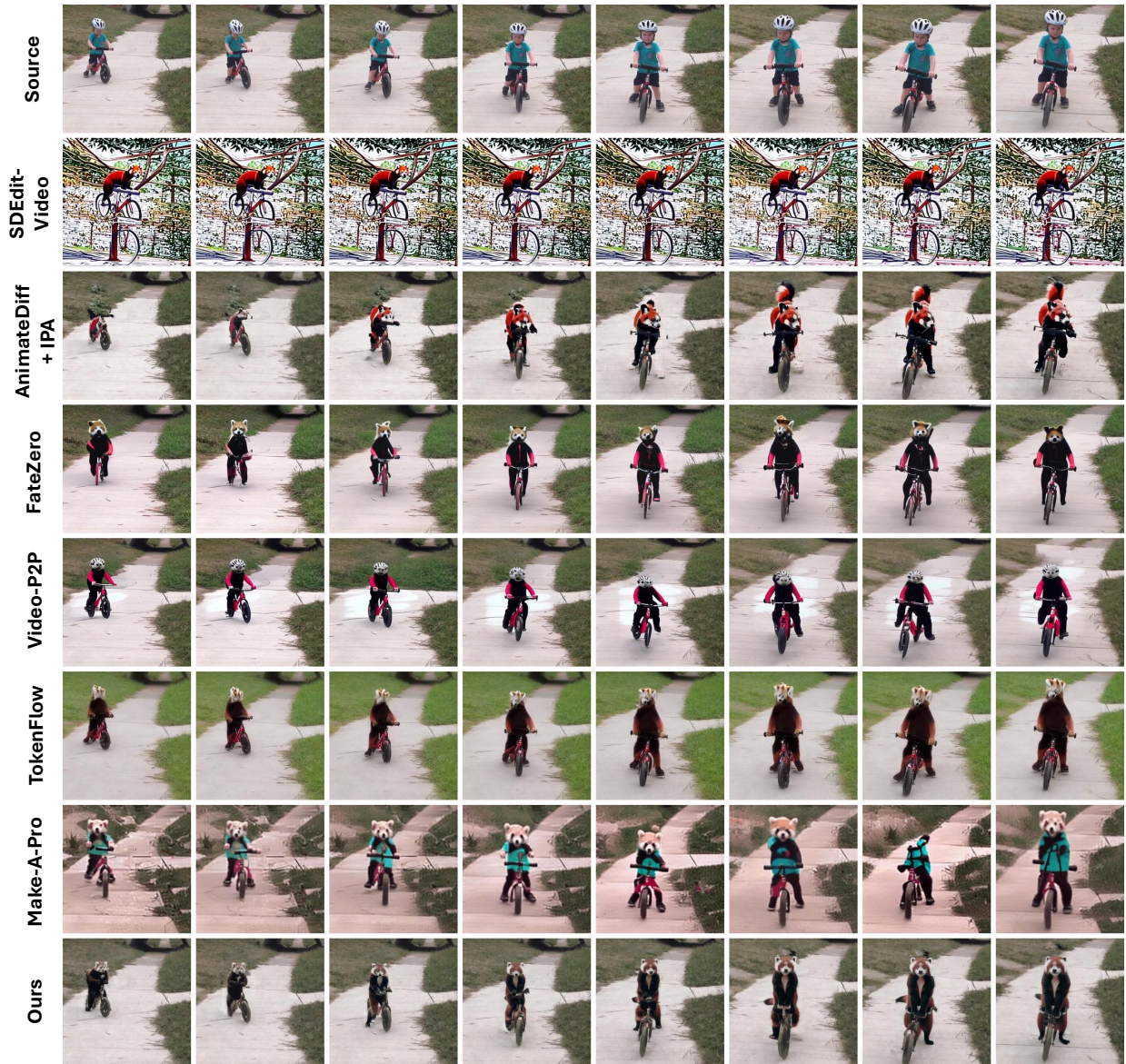


Figure 16. **Complete video editing comparisons with baseline methods.** FateZero [30] and Make-a-Pro [50] use text prompts generated by BLIP-2 [20] following their respective proposed strategies. TokenFlow [11], Video-P2P [23], FateZero [30], and SDEdit-Video [24] use only text prompts, while Make-a-Pro [50], AnimateDiff [13]+IP-Adapter [46], and our proposed method use both image and text prompts.

"a ~~guy~~ bear floating with kiteboard"



Figure 17. **Complete video editing comparisons with baseline methods.** FateZero [30] and Make-a-Pro [50] use text prompts generated by BLIP-2 [20] following their respective proposed strategies. TokenFlow [11], Video-P2P [23], FateZero [30], and SDEdit-Video [24] use only text prompts, while Make-a-Pro [50], AnimateDiff [13]+IP-Adapter [46], and our proposed method use both image and text prompts.

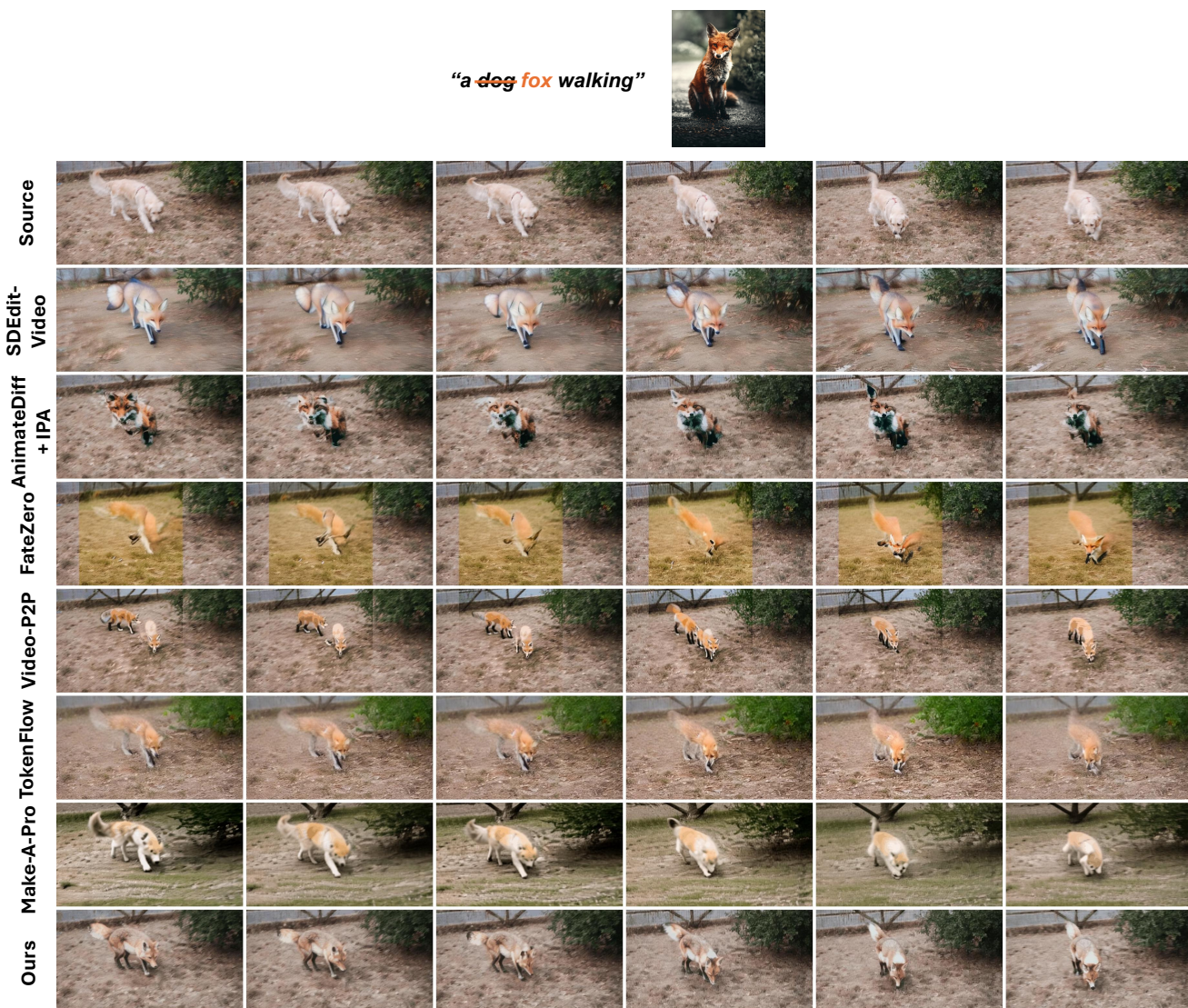


Figure 18. **Complete video editing comparisons with baseline methods.** FateZero [30] and Make-a-Pro [50] use text prompts generated by BLIP-2 [20] following their respective proposed strategies. TokenFlow [11], Video-P2P [23], FateZero [30], and SDEdit-Video [24] use only text prompts, while Make-a-Pro [50], AnimateDiff [13]+IP-Adapter [46], and our proposed method use both image and text prompts.



Figure 19. **Complete video editing comparisons with baseline methods.** FateZero [30] and Make-a-Pro [50] use text prompts generated by BLIP-2 [20] following their respective proposed strategies. TokenFlow [11], Video-P2P [23], FateZero [30], and SDEdit-Video [24] use only text prompts, while Make-a-Pro [50], AnimateDiff [13]+IP-Adapter [46], and our proposed method use both image and text prompts.